

# Hollow cathode ion lasers for deep ultraviolet Raman spectroscopy and fluorescence imaging

M. C. Storrie-Lombardi<sup>a)</sup>

*Jet Propulsion Laboratory, California Institute of Technology, MS 183-301-4800 Oak Grove Dr., Pasadena, California 91109*

W. F. Hug

*Photon Systems, Inc., 1512 Industrial Park Street, Covina, California 91722*

G. D. McDonald, A. I. Tsapin, and K. H. Nealon

*Jet Propulsion Laboratory, California Institute of Technology, MS 183-301-4800 Oak Grove Dr., Pasadena, California 91109*

(Received 15 May 2000; accepted for publication 5 March 2001)

This article describes the development of hollow cathode ion lasers and their use in constructing an ultraviolet micro-Raman spectrograph with native fluorescence imaging capability. Excitation at 224.3 nm is provided by a helium–silver hollow cathode metal ion laser and at 248.6 nm by a neon–copper hollow cathode metal ion laser. Refractive microscope objectives focus chopped continuous wave laser light on a sample and collect 180° scattered photons. Imaging is accomplished by broadband visible illumination and by deep ultraviolet laser induced excitation of visible wavelength native fluorescence in untagged micro-organisms. This makes possible a detection strategy employing rapid imaging with laser excitation to locate regions of native fluorescence activity, followed by deep ultraviolet resonance Raman spectroscopy of the identified fluorescent sites. We have employed this probe for *in situ* detection of micro-organisms on mineral and soil substrates. We present here the deep ultraviolet resonance Raman spectra for the gram negative iron reducing bacterium *Shewanella oneidensis* obtained while the micro-organism remains *in situ* on the unpolished surface of the mineral calcite and in a Mars soil analog, JSC1. In the current configuration the *in situ* mineral surface limit of detection for fluorescence is one organism in  $2 \times 10^4 \mu\text{m}^2$  field of view and of order 20–30 micro-organisms for Raman spectra. For the Mars soil sample analog fluorescent target selection gives an effective ultraviolet resonance Raman spectral detection limit of  $6 \times 10^4$  cells/gm or  $\sim 60$  ppb. © 2001 American Institute of Physics. [DOI: 10.1063/1.1369627]

## I. INTRODUCTION

Detection and identification of sparsely distributed yet spatially localized concentrations of micro-organisms is a fundamental task common to *in situ* detection of life on Mars, planetary contamination containment, forensic investigation, and biological warfare countermeasures.<sup>1</sup> The goals for each of these efforts are best accomplished with minimal sample preparation including the avoidance of tagging molecules. Among optical techniques, fluorescence remains the gold standard for sensitivity.<sup>2</sup> However, as usually implemented it has either depended on the introduction of fluorescent tags or the serendipitous presence of a chromophore molecule with strong absorption bands at visible wavelengths. A variety of ring compounds essential to micro-organisms on this planet, including the aromatic amino acids and the nucleic acids, exhibit strong native fluorescence response to excitation between 200 and 280 nm.<sup>3,4</sup> Broadband mercury lamp UV excitation has been employed to elicit native fluorescent activity in the bacterium *E. coli*<sup>5</sup> and

fungi.<sup>6</sup> Excitation at 230 nm produces detectable native fluorescence activity in algae and phytoplankton.<sup>7</sup> Detection sensitivity is dependent on both total photon flux and target molecule cross section. However, although native fluorescence response might serve as an initial detection probe, it often provides little specificity to aid in the identification of a target.

Raman spectroscopy, first demonstrated by Raman and Krishnan in 1928, is a vibrational spectroscopy technique measuring the frequency shifts produced by the inelastic scattering of light from a target molecule.<sup>8</sup> The high information content of the spectra, the nondestructive nature of the technique, and the ease of sample preparation have made Raman spectroscopy extremely attractive for monitoring a wide variety of biochemical reactions,<sup>9,10</sup> determining the molecular structure of viruses,<sup>11–19</sup> and characterizing terrestrial soil and mineral samples.<sup>20</sup> The technique has been proposed for *in situ* mineralogical and paleontological exploration of the Martian regolith.<sup>21,22</sup>

Unfortunately, the Raman event is an inefficient phenomenon [signal to noise ( $S/N < 10^{-9}$ )]. Under controlled laboratory conditions deep UV laser excitation within the absorption bands (200–280 nm) of the nucleic acids, aro-

<sup>a)</sup> Author to whom correspondence should be addressed; electronic mail: mcs1@dna.jpl.nasa.gov

matic amino acids, and quinones can produce *resonance* Raman events increasing signal strength by as much as  $10^8$ .<sup>23</sup> As a result, several laboratories have used UV resonance Raman (UVR) spectroscopy to investigate nucleic acids,<sup>24,25</sup> the secondary structure of DNA,<sup>26–29</sup> and the aromatic amino acids.<sup>30–35</sup> Reliance on the resonance event to achieve adequate S/N levels minimizes interference from neighboring potentially Raman-active molecular species with absorption bands distant from the exciting wavelength. Such selective UVR has proven quite useful in monitoring alterations in oxidation state, electronic excited states, and peptide conformation.<sup>36–47</sup> Early attempts to produce nonresonant Raman spectra of bacteria with visible light excitation were unsuccessful due to fluorescence interference.<sup>48–52</sup> More recently excitation in the 200–257 nm range has produced UV resonance Raman spectra for a variety of bacteria and spores.<sup>53–58</sup>

The routine use of deep UV excitation of aromatic amino acid and nucleic acid species to obtain native fluorescence and resonance Raman signatures *in situ* has been dependent on the development of a lightweight laser light source emitting photons in the 200–250 nm range. Hollow cathode ion lasers, first demonstrated at the University of Budapest in 1974,<sup>59</sup> have several unique properties that make them ideal for *in situ* UV laser induced fluorescence and Raman spectroscopy. Among these features are an array of emission wavelengths including 224.3 nm from a helium charge exchange pumped sputtering silver hollow cathode laser and 248.6, 260.0, and 270.3 nm from a neon charge exchange pumped sputtering copper hollow cathode laser. The linewidth of all of these emission lines is less than  $0.1 \text{ cm}^{-1}$ . Excitation at 248.6 nm falls within the absorption bands for primarily the nucleic acids and to a lesser extent the aromatic amino acids. Excitation at 224.3 nm falls within the absorption bands for the aromatic amino acids. The early development of these lasers was hampered by the lack of durable low scatter and low absorption laser mirror coatings resistant to optical damage. Recognized as an efficient source of deep UV laser light, the development of this technology continued at a handful of academic and industrial sites.<sup>60–62</sup>

In this report we describe such lasers and outline the optical path for the compact deep UV imaging and spectroscopy system we have constructed for *in situ* sample analysis. We next discuss the native fluorescence and resonance Raman response of the aromatic amino and nucleic acids to excitation in the deep ultraviolet at 224.3 and 248.6 nm. We illustrate the system's potential utility by presenting UVR spectra for the gram negative iron reducing bacterium *Shewanella oneidensis* (MR-1) obtained *in situ* with the organism residing (a) on the unpolished surface of the mineral calcite and (b) in a medium-grained Mars soil analog.

## II. INSTRUMENTATION

### A. Ultraviolet lasers

The lasers presented here differ significantly from other metal vapor lasers in that the metal vapor pressure is generated by sputtering of a metal cathode rather than by evaporation from a hot metal source. Hollow cathode sputtering

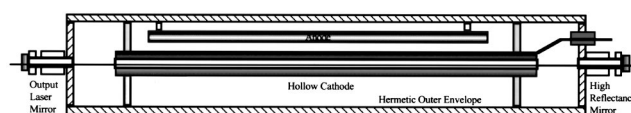


FIG. 1. Schematic representation of a hollow cathode metal ion laser.

metal ion lasers operate at room temperature, require no preheating or standby power, emit laser output within about  $20 \mu\text{s}$  after application of voltage to the laser tube, and require an average input power of 20–100 W. An advantage of hollow cathode laser technology over positive column lasers is that the discharge can be modulated with fast rise and fall time less than  $5 \mu\text{s}$ . Therefore the output and input power can be varied in an approximate linear fashion to suit experimental requirements. For *in situ* nondestructive biosignature detection the lasers operate at 1% duty cycle to minimize heating effects. The pulse width of the laser output can be varied from a few microseconds to a millisecond or more since the laser transitions are continuous wave (cw).

The lasers used in this study produce an oscillation bandwidth of less than 3 GHz, giving a limiting Raman resolution due to laser emission bandwidth of approximately  $0.1 \text{ cm}^{-1}$ . The 224.3 nm laser (HeAg) uses a combination of helium and other noble gases as buffer gases and very pure silver on the inner diameter (Fig. 1) as the gain material (Photon Systems, Model HeAg60-224SL). The 248.6 nm laser (NeCu) uses a combination of neon and other noble gases as buffer gases and very pure copper as the gain material (Photon Systems, Model NeCu60-248SL). The discharge geometry for both lasers is transverse with a brush-type anode located along most of the length of the 40-cm-long by 3-mm inside diam cathode.

Although the 224.3 and 248.6 nm emission lines are cw transitions, we operate these lasers in a chopped cw fashion to reduce average input power and minimize the size and complexity of the laser tube and power supply. Optimum peak output is over 400 mW for NeCu laser and 100 mW for HeAg lasers with an operating duty cycle of about 1% (overall length 56 cm; active gain length 40 cm). The average input power to the laser is less than 100 W. A power supply provides square wave voltage pulses to the cathode with a pulse width adjustable from about 30 to  $500 \mu\text{s}$ . The corresponding drive current is also square wave and ranges in current from about 5 to 30 A. Laser output commences within  $\sim 10 \mu\text{s}$  of voltage application. Each laser pulse is independent, allowing the laser to operate in single pulse or multiple pulse mode. The laser can be operated in extreme environments without the need for warm-up, preheating, or temperature regulation. The emitted laser beam is  $\sim 3 \text{ mm}$  diameter with a divergence  $\sim 0.3 \text{ mr}$ . The longitudinal mode spacing is  $\sim 257 \text{ MHz}$ . The transverse mode structure is multimode with the ‘‘times diffraction limit’’ of the beam about 18. Hence, these lasers can be focused to spot sizes of  $\sim 5 \mu\text{m}$  using an objective lens with numerical aperture (NA) = 0.5.

The system includes a 325.0 nm cw laser for instrument alignment. The 325.0 nm laser is a positive column metal vapor laser using helium as a buffer gas and cadmium as the active gain material (Melles Griot, P/N 3056-5). This laser

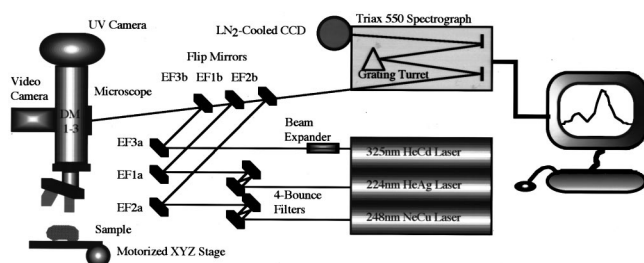


FIG. 2. Optical layout of the deep UV native fluorescence imaging and resonance Raman spectroscopy system.

requires a warm-up time of about 5 min. Output of this laser is  $\sim 5$  mW. The transverse mode is a Gaussian with a diameter of about 0.2 mm.

## B. Optical design

The UV Raman instrument is illustrated in Fig. 2. It is composed of a spectrograph, a charge coupled device (CCD) array detector, three separate ultraviolet lasers, a microscope with multiple incoherent and coherent sources, a three axis motorized stage, a CCD video camera, a UV camera, and assorted lenses, spatial filters, edge filters, dichroic mirrors, and other optics. The instrument was designed to allow excitation at three wavelengths in the ultraviolet. Excitation wavelength can be changed within a few seconds using flip mirrors and a dichroic mirror slide.

The optical path for each excitation wavelength is similar. At the output of the HeAg and NeCu lasers are multi-bounce edge filters employed to reduce plasma line emission from the lasers. The minimal plasma line emission of the HeCd laser makes possible the use of only a beam expanding lens pair. After passing through the multi-bounce filter (or beam expander), the laser beam is reflected in tandem by two edge filters (Barr Associates), EFa and EFb. The edge filters are fabricated to efficiently reflect the laser wavelength and transmit at wavelengths immediately above the laser wavelength. Thus, EF1b is designed for 224.3 nm, EF2b for 248.6 nm, and EF3b for 325.0 nm. These filters also assist in eliminating unwanted laser plasma emission lines. EFa and b are identical edge filters and are used in pairs to bring the laser beams into alignment with the optical path from the microscope entrance axis. The EFb filters are mounted on flip-mirror assemblies (New Focus, P/N 9891) to allow rapid change of excitation wavelength. After reflection by EFb, the laser beam is directed into the microscope. Within the microscope is a dichroic mirror slide containing three dichroic mirrors, DM1, DM2, and DM3, each designed to efficiently reflect, at  $45^\circ$ , the laser line and a wavelength interval about 20 nm above the laser line. DM1 is for the 224.3 nm laser (CVI, P/N TLM1-240-45-1025), DM2 is for the 248.6 nm laser (CVI, P/N KRF-1025-45), and DM3 is for the 325.0 nm laser (CVI, P/N N-1025-45). Laser excitation wavelength can easily be selected by choosing the EFb and DM mirrors corresponding to the desired wavelength.

The microscope objective is a  $40\times$  ultraviolet refractive lens (Optics for Research, LMU-40) with effective focal

length of 5 mm, working distance of 1 mm, NA of 0.50, and entrance aperture of 5 mm coated for UV between 224 and 325 nm with overall transmission of  $>92\%$ . Calculated spot diameters at the sample for this lens are 2.85, 3.16, and  $4.14 \mu\text{m}$  for the 224, 248, and 325 nm lasers, respectively. The Rayleigh Range ( $R_r$ ) defined as one half the depth of focus is the distance above and below the focal plane where the beam diameter has expanded to 1.414 times the minimal spot diameter and the power deposition per unit area is one half that at the focal plane. For 224, 248, and 325 nm  $R_r$  is 28.5, 31.5, and  $41.4 \mu\text{m}$ , and power delivered to the sample is 100, 480, and  $330 \mu\text{W}$ , respectively. To minimize the total UV dose/unit time to sample the system employs a motorized XYZ microscope stage moving the target material  $0.4 \text{ mm/s}$ . Target trajectory can be preprogrammed or altered in real time via computer interface (Newport Corporation, ESP6000 Unidrive6000).

The microscope axis is vertical with the laser beam reflected by one of the three DM mirrors, directed downward into the entrance aperture of the objective lens, and focused on the sample (Fig. 1). Above DM is a microscope relay lens (Edmund Scientific, H37820) which images the sample onto a  $768\times 494$  element, 0.003 LUX, B/W CCD video camera (Watec, WAT-902B). Pixel size of the CCD camera is  $8.4 \mu\text{m}(\text{horizontal})\times 9.8 \mu\text{m}(\text{vertical})$ . Spatial resolution of the CCD video camera is about  $0.1 \mu\text{m}$  per pixel using the  $40\times$  refracting objective lens.

The camera produces images using broadband visible illumination (transmission or reflectance) and visible wavelength fluorescence from laser excitation at 325.0, 248.6, or 224.3 nm. The two visualization modes make it possible to locate fluorescent targets against irregular soil or mineral backgrounds. Using EFa and EFb mirrors, the laser beam spot can be centered in the middle of the video image.

Scattered light from the excited region on the sample is collected by the objective lens and collimated along the optical path to the spectrograph. The EF filters reject Rayleigh scattered light at the excitation wavelength. The remaining light, devoid of plasma lines and scattered light is then focused by L3 onto the entrance slit of the spectrograph. The diameter of the beam of scattered light from the sample is 8 mm, using the  $40\times$  refractive objective. For compatibility with the etendue (the product of the solid angle and aperture area) of the spectrograph, the focal length of L3 is 75 mm. With this lens a minimum spectrograph slit width of  $125 \mu\text{m}$  is needed to minimize light loss.

The spectrograph is a 0.55 m,  $f/6.4$  fully automated Czerny–Turner imaging spectrograph (Instruments SA, TR550MST1) with both 1800 and 3600 g/mm low stray light holographic gratings ( $76 \text{ mm}\times 76 \text{ mm}$  each) in a triple grating turret. The turret, entrance slits, and shutter are all computer controlled. The CCD array detector assembly uses a  $2048\times 512$  array of  $13.5 \mu\text{m}$  square pixels back illuminated and UV anti-reflection coated detector (English Electric Valve) temperature regulated and mounted in a liquid nitrogen cooled Dewar (Instruments SA, Spectrum One CCD-2048 $\times$ 512-4). The dispersion of the spectrograph is  $0.516 \text{ nm/mm}$  with the 3600 g/mm grating and  $1.032 \text{ nm/mm}$  with the 1800 g/mm grating. With the above CCD array

TABLE I. Wave number coverage of the spectrograph. Wavelength coverage depends on both excitation wavelength (224, 248, or 325 nm) and choice of grating (1800 or 3600 grooves per millimeter).

Grating	1800 g/mm		3600 g/mm	
	Resolution/pixel	Single capture	Resolution/pixel	Single Capture
224 nm	2.78 cm <sup>-1</sup>	5686 cm <sup>-1</sup>	1.39 cm <sup>-1</sup>	2844 cm <sup>-1</sup>
248 nm	2.27 cm <sup>-1</sup>	4641 cm <sup>-1</sup>	1.13 cm <sup>-1</sup>	2320 cm <sup>-1</sup>
325 nm	1.32 cm <sup>-1</sup>	2702 cm <sup>-1</sup>	0.66 cm <sup>-1</sup>	1351 cm <sup>-1</sup>

detector the resolution is therefore 0.00697 nm per pixel using the 3600 g/mm grating and 0.01393 nm per pixel using the 1800 g/mm grating. The wavelength coverage in one capture is 14.27 nm with the 3600 g/mm and 28.53 nm with the 1800 g/mm grating (Table I). The dark charge of this CCD detector is <1 e/pixel/h. Readout register full well capacity is typically 600 000 e and readout noise is typically 3 e rms.

### III. EXPERIMENTAL CONDITIONS

Initial system tests have employed a gram negative bacteria *Shewanella oneidensis*, a facultative anaerobe  $\sim 1 \times 2 \mu\text{m}$  in length common to many terrestrial and marine environments.<sup>63</sup> Cultures were grown in LB medium at room temperature in the microbiology laboratory of the Center for Life Detection (Jet Propulsion Laboratory, California Institute of Technology). Harvested cells were centrifuged and re-suspended in double distilled water to remove culture medium. Cell concentrations ranged from  $10^6$  to  $10^8$  cells/ml. Aliquots of these suspensions or dilutions of them were then added to mineral and soil backgrounds including a  $1.0 \times 1.2$  cm unpolished calcite (calcium carbonate) crystal and granular palagonite.

On Earth calcium carbonate structures imply hydrothermal and sedimentary geological activity and make excellent environments for mixed colonies of micro-organisms. Calcite exhibits a large Raman cross section with vibrational modes at 1086–1088 cm<sup>-1</sup> (primary) 713, 1435, and 1749 cm<sup>-1</sup>. Although the actual composition of Martian soil remains unknown, palagonite from the Muana Kea volcano in Hawaii provides the best known spectral analog.<sup>64–67</sup> Palagonite exhibits no native fluorescence or resonance Raman emission for the power densities and excitation wavelengths employed in this study.

Calcite samples were cleaned with triple ethanol washes and palagonite samples were baked at 500 °C. Base line spectra were obtained at 325, 248, and 224 nm on all samples prior to inoculation with micro-organisms. Wash and autoclave protocols were repeated if these spectra indicated contamination subsequent to cleaning. For the calcite experiment 20–80  $\mu\text{L}$  aliquots of the bacterial suspensions were added to a 0.5 cm area on a moderately smooth calcite face. For the palagonite experiment similar aliquots were added to 80–100 mg of dry powdered palagonite, allowed to dry, and then mixed in a 0.5-cm-diam depression in a quartz microscope slide. Samples were visually scanned in video mode for evidence of localized laser induced native fluorescence response to 325, 248, and 224 nm excitation. Frame rates were 1/30 s. UVRR spectra were obtained with excitation at

325, 248, and 224 nm. Power delivered to sample at each wavelength was 0.24, 0.33, and 0.14 mW, respectively. The lasers were defocused to minimize sample damage resulting in a spot size approximately 80  $\mu\text{m}$  in diameter. Data acquisition was accomplished both in scanning mode moving across the target area at 0.4–1.0 mm/s and as single area collections focused on fluorescing or nonfluorescing regions. No evidence of sample damage was detected in the collected spectra for scanning or single spot collections of 1 min duration or less. Spectra data collection times ranged from 10 to 60 s with 30–60 s sufficient to elicit reproducible spectra for bacterial samples. Data are displayed in counts per minute.

### IV. RESULTS

Figure 3 depicts the UV Raman spectra for cleaned calcite and calcite inoculated with *S. oneidensis*. In Fig. 3(a) Raman vibrational modes for calcite appear only at 1086 cm<sup>-1</sup> for 325 nm excitation (fluorescence obscures the remaining modes). Activity appears at 713, 1086, 1430, and 1735 cm<sup>-1</sup> for 248 nm excitation [Fig. 3(b)] and at 1086 (primary), 1428, and 1725 cm<sup>-1</sup> using 224 nm excitation [Fig. 3(c)]. At 325 nm excitation of calcite inoculated with bacteria [Fig. 3(d)] all bacterial modes appear obscured in fluorescence with only the strong primary calcite line clearly resolved. Vibrational modes for *S. oneidensis* appear at 1338, 1427, and 1612 cm<sup>-1</sup> for 248 nm excitation [Fig. 3(e)] and at 765, 1007, 1186, 1344, 1554, and 1600 cm<sup>-1</sup> for 224 nm excitation [Figure 3(f)]. The Raman event and appropriate assignment of these modes depends on molecular ring breathing, stretch, and bending phenomena and, for the very low powers employed in this experiment, a significant reso-

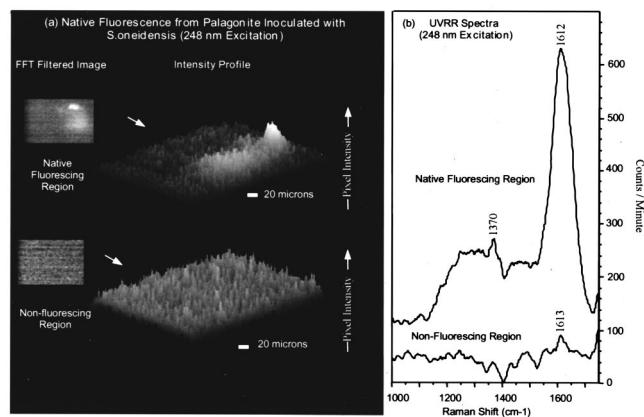


FIG. 3. Ultraviolet (excitation at 325, 248, and 224 nm) resonance Raman spectra of calcite [(a), (b), and (c)] and calcite inoculated with the bacteria *S. oneidensis* [(d), (e), and (f)]. Collection time is 60 s.

TABLE II. Assignments of expected strong resonance Raman bands contributing to UVRR spectra of *S. oneidensis*.<sup>a</sup>

Molecule	Raman band assignment
Tryptophan	<u>757–762</u> <sup>a</sup> symmetric stretch of benzene and pyrrole rings [224]
	877–880 in-plane deformation
	<u>1006–1016</u> symmetric stretch of benzene and pyrrole rings [224]
	<u>1340–1350</u> a pyrrole ring vibration [224]
	<u>1549–1555</u> symmetric stretching of the indole ring [224]
Tyrosine	<u>1614–1622</u> phenyl ring vibration [224/248]
	830–832 Fermi resonance doublet
	850–853 symmetric ring stretch
	<u>1178–1180</u> in-plane CH bend [224]
Guanine <sup>b</sup>	<u>1613–1617</u> in-plane ring stretching [224/248]
	<u>1322–1326</u> (N7C8 s <sup>c</sup> ; C8H b <sup>d</sup> ) purine ring bonds [248]
	<u>1485–1489</u> (C8H b; C8N9, C8N9, N7C8 s) purine ring bonds
	1575–1580 (N3C4, C4C5, C5N7 s) ring mode stretching
	1603 (N1H b, C2N s) in-plane bending and ring stretching [248]
Adenine	<u>1336–1339</u> (C5N7, N7C8 s) purine ring bonds [248]
	1482–1485 (C4N9 s, C8H b) purine ring bonds
	1580–1581 (C4C5, N3C4 s) ring mode stretching
Cytosine	<u>1527–1528</u> (N3C4, N1C2 s) ring mode stretching [224]
	1650 (C2=O, C2N3 s) in-plane bending and ring stretching

<sup>a</sup>Raman band frequencies are in  $\text{cm}^{-1}$  units. Assignments, frequency ranges and nomenclature are from experimental and model compound studies using excitation between 223 and 229 and 244 and 248 nm (see Refs. 25, 29–33, and 68).

<sup>b</sup>Nucleic acid studies employed nucleotides, deoxynucleosides, or the duplexes poly(rA)-poly(rU) and poly(dG-dC). Abbreviations signify Raman.

<sup>c</sup>stretching and

<sup>d</sup>bending modes. The most prominent bands are in bold. Regions exhibiting significant activity in the present study are underlined and the excitation frequencies responsible for the UVRR response appear in bold between square brackets [ ].

nance enhancement must occur in ring structures, carbon-carbon double bonds, carbonyl bonds, and amides. The most common molecular sources in microbial cells are the aromatic amino and nucleic acids. The assignments for the major bands characterizing the aromatic amino and nucleic acids have been well studied for UVRR with excitation wavelengths between 200 and 257 nm using both cw and pulsed lasers.<sup>25,29–33,68</sup> With minor exceptions the major bacterial spectral contributions at the wavelengths and powers employed derive from the aromatic amino acids tryptophan and tyrosine plus three of the bases, adenine, guanine, and cytosine. Phenylalanine, thymine, and uracil exhibit cross sections an order of magnitude smaller than these five molecules. Table II summarizes the most prominent bands characteristic of these molecules for excitation between 223 and 229 and 244 and 248 nm. Modes detected in our experiment are underlined and the exciting laser wavelength appears in square brackets. Nelson and colleagues have reviewed the assignment of vibrational bands in whole cell bacteria.<sup>56</sup>

In our experiments tryptophan exhibits a particularly large cross section for both native fluorescence and UV resonance Raman activity with both 224.3 nm and 248.6 nm excitation. Activity with 224.3 nm excitation at  $1554 \text{ cm}^{-1}$  can be assigned to symmetric stretching of tryptophan's indole ring. Modes at 1007 and  $765 \text{ cm}^{-1}$  are assigned to a symmetric

stretch of benzene and pyrrole rings within the indole structure. Activity at  $1344 \text{ cm}^{-1}$  arises from tryptophan pyrrole ring vibration. The response to 224 nm excitation at  $1600 \text{ cm}^{-1}$  probably arises from a tryptophan phenyl ring vibration and tyrosine in-plane ring stretching. The mode appearing at  $1186 \text{ cm}^{-1}$  most likely originates from tyrosine in-plane CH bend.

With excitation at 248.6 nm the activity at  $1338 \text{ cm}^{-1}$  can be assigned to purine ring bonds. The activity at  $1612 \text{ cm}^{-1}$  most likely arises from purine in-plane bending and ring stretching as well as tryptophan phenyl ring vibration. The exact origin of the response at  $1427 \text{ cm}^{-1}$  remains unclear, but most likely arises from purine ring bonds.

The variation in peak locations produced by excitation at 224.3 and 248.6 nm reflects the selective nature of the resonance Raman experiment. For example, the shift between  $1600$  and  $1612 \text{ cm}^{-1}$  for 224.3 and 248.6 nm excitation respectively, may reflect a shift in relative resonance Raman cross sections for the  $1603 \text{ cm}^{-1}$  tyrosine *v8b* mode. The relative increase in tyrosine cross section with 224 nm excitation is also reflected in the appearance of the  $1186 \text{ cm}^{-1}$  band. The activity at 1007 and  $1554 \text{ cm}^{-1}$  during 224.3 nm excitation is absent as expected at 248.6 nm excitation if it arises from tryptophan symmetric ring stretch.

To estimate instrument sensitivity for eliciting spectral signatures of micro-organisms on a mineral surface, 10–40  $\mu\text{L}$  aliquots of suspensions containing  $10^7$ – $10^8$  organisms/ml were inoculated onto a 0.5-cm-diam region of a moderately smooth but unpolished calcite face. Equal aliquots were placed on a standard microscope. Cells were counted on the microscopic slides using both phase contrast and fluorescence images obtained with a standard laboratory epifluorescence microscope (Nikon, Eclipse E600) and then on our test instrument using confocal visible wavelength and fluorescence images. A >99% congruence for micro-organism detection existed between the two broadband white light transmission techniques (phase contrast and confocal) and native fluorescence images. The detection of single organisms by native fluorescence imaging in the test instrument was accomplished with an effective field of view of  $\sim 2$ – $5 \times 10^3 \mu\text{m}^2$  (50–80  $\mu\text{m}$  laser beam diameter).

Raman spectra of the inoculated calcite region revealed strong vibrational modes at  $1600 \text{ cm}^{-1}$  for 224 nm excitation and at  $1612 \text{ cm}^{-1}$  with 248 nm excitation. Peak heights were plotted as a function of the average number of organisms expected to fall within the excitation beam during scanning. Figure 4 demonstrates the expected signal falloff as a function of dilution with complete loss of signal (1 min integration) occurring when cell densities fell below 5–10 cells per  $100 \mu\text{m}^2$ .

Spectra obtained by random scanning of the calcite surface gave evidence of signal strength variability at all dilutions. Examination of visual and fluorescent microscopic images revealed a nonrandom distribution of micro-organisms across the relatively rugged calcite surface. Bacteria tend to accumulate along crevasses in the mineral leaving a patchy target for the relatively small UV laser spot size. This phenomenon manifested in the inoculated samples mimics the behavior of micro-organisms in natural environments with

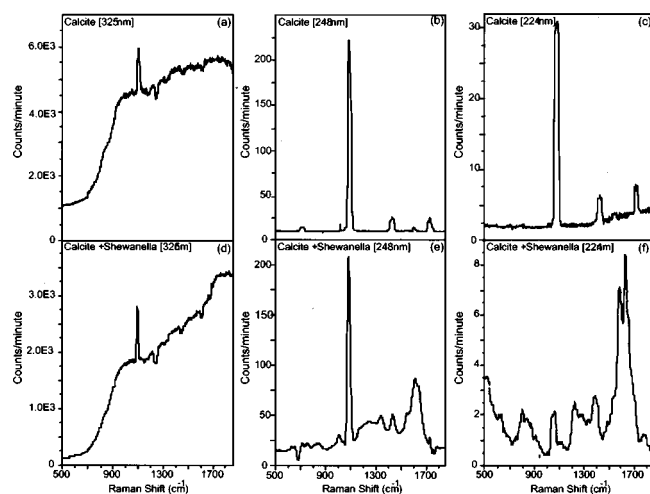


FIG. 4. UV resonance Raman peak intensities as a function of the average number of bacteria expected in a  $50 \mu\text{m}$  beam. Aliquots of cells were inoculated onto a natural calcite surface. Excitation was at  $224 \text{ nm}$  ( $\circ$ ) and  $248 \text{ nm}$  ( $+$ ).

cells clustering in localized niches meeting specific nutrient, water, mineral, and energy requirements. As the mean distance between clusters of organisms increases with increasing dilutions, the efficiency of random scanning diminishes. Visual observation of fluorescent activity made it possible to collect spectra from both fluorescing and nonfluorescing regions. Fluorescing areas ranged in size from  $5$  to  $15 \mu\text{m}$  in diameter giving an equivalent two-dimensional target cross section of  $\sim 20$ – $200$  cells. UVRR spectra obtained using  $248.6$  and  $224.3 \text{ nm}$  excitation of nonfluorescing regions produced only the classical calcite modes, with no evidence of a biological signature [similar to spectra in Figs. 3(b) and 3(c)]. In contrast, the regions exhibiting clusters of native fluorescence yielded spectra compatible with the presence of micro-organisms [similar to spectra in Figs. 3(e) and 3(f)].

A similar approach was employed with the Mars soil analog. Palagonite was inoculated with varying numbers of bacterial cells. Final soil concentrations of bacteria were calculated to range between  $6 \times 10^4$  and  $3 \times 10^5$  organisms/gm. Samples were then scanned with  $248.6 \text{ nm}$  excitation to identify fluorescing and nonfluorescing areas. Fluorescence emission in visible wavelengths again allowed identification of fluorescing regions using real time video. Following classification of a region by its fluorescent activity Raman spectra were collected from both fluorescing and nonfluorescing regions. The  $1612 \text{ cm}^{-1}$  line elicited by  $248 \text{ nm}$  excitation was the strongest and most robust signal. Table III compares the magnitude of the  $1612 \text{ cm}^{-1}$  line with estimated concentration of organisms per milligram of soil. While all areas gave evidence of organism inoculation, signal strength from fluorescing regions was  $5$ – $35$  times stronger than the signal from nonfluorescing soil. Native fluorescence regions were observed to cover  $10\%$ – $20\%$  of the laser spot size. Calculations for a two-dimensional tiling of organisms predict that the majority of spectral information derives from  $\sim 20$ – $40$  cells located in the center of the laser excitation.

Figure 5 depicts the native fluorescence image [Fig.

TABLE III. Dependence of UVRR signal strength for *S. oneidensis* in the presence of fluorescence activity after  $248 \text{ nm}$  excitation. Varying quantities of the micro-organism were inoculated into  $80$ – $100 \text{ mg}$  of a palagonite Mars soil analog. UVRR signal at  $1604 \text{ cm}^{-1}$  appears in all samples, but proves dependent primarily in the presence or absence of localized fluorescence instead of on total number of organisms introduced. Peak intensities were converted to signal to noise ratios, i.e.,  $S/N=10$  implies the peak height is an order of magnitude greater than the noise level for this spectral region. Effective detection level is calculated as  $6$ – $30 \times 10^4$  cells/gm or  $6$ – $30 \text{ ppb}$  of the palagonite samples.

Organism concentration	Peak intensity ( $1604 \text{ cm}^{-1}$ ) with $248 \text{ nm}$ excitation (S/N)	
	Nonfluorescing region	Fluorescing region
Cells/mg of soil		
305	10	55
94	5	75
62	7	235

5(a)] and the accompanying UVRR spectra [Fig. 5(b)] for a region of palagonite exhibiting native fluorescence and a nonfluorescing region. The region producing spatially localized native fluorescence yields an UVRR spectral signal strength some two orders of magnitude greater than the nonfluorescing portion of the sample. The data imply that rapid image scans of a sample to identify regions of native fluorescence can provide localized target areas appropriate for spectral data collection. Calculations derived from the number of cells added to the  $80$ – $100 \text{ mg}$  of soil produce an effective detection in this study of  $6 \times 10^4$  cells/gm or about  $60$  parts per billion (ppb) assuming a total weight for one micro-organism  $\sim 10^{-12} \text{ gm}$ .<sup>69</sup>

## V. DISCUSSION

Hollow cathode sputtering metal ion lasers emitting at  $224.3$  and  $248.6 \text{ nm}$  have made it possible to elicit *in situ*

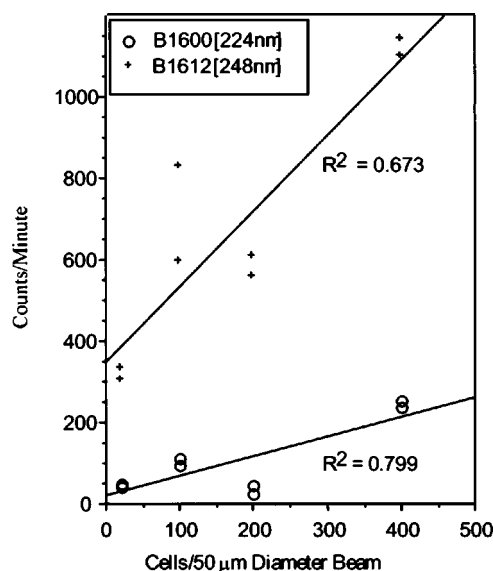


FIG. 5. Native UV fluorescence and resonance Raman spectra for palagonite inoculated with *Shewanella oneidensis*. A region evidencing a spatially localized region of native fluorescence activity exhibits a significant increase in resonance Raman spectral S/N at  $1612$ – $1613 \text{ cm}^{-1}$  when compared to a relatively nonfluorescing region. Excitation is at  $248 \text{ nm}$  and collection time was  $60 \text{ s}$ .

native fluorescence and a resonance Raman spectral signature from the bacterium *Shewanella oneidensis* on a mineral (calcite) surface and a Mars soil analog (JSC-1). The origin of both the native fluorescence activity and the UVRR spectrum can be tentatively assigned to bacterial nucleic and aromatic amino acids. In current configuration a relatively diffuse large beam configuration has been employed to diminish sample damage and increase the efficiency of wide area rapid search for clusters of native fluorescence. Obtaining spectra from these native fluorescent clusters sparsely dispersed in a soil sample produces effective detection limits for the spectral signature of tens of parts per billion. Laser spot size is diffraction limited making it theoretically possible to extract spectral information from a 3–5  $\mu\text{m}^2$  region. Focusing laser power in this fashion would permit the interrogation of a single organism, but at the cost of significantly increasing search time.

Other extreme environment targets for this system include residual pigments that remain following the death of a micro-organism. These are often comprised of relatively insoluble organic ring structures, but typically derive from tryptophan, tyrosine, and/or phenylalanine. Native fluorescence imaging and wavelength selective Raman spectral interrogation of these difficult to analyze compounds could be the most direct observational technique available to us during extended extreme environment missions.

It is now feasible to fabricate hollow cathode metal ion deep UV lasers 10–15 cm in length, 2–4 cm in diameter, weighing 50–100 g with an electronics package of comparable size, and drawing only 2–3 W of electrical power. This technology makes possible the development of portable ultraviolet fluorescence imaging and Raman spectral probe for the geobiological exploration of terrestrial and extraterrestrial natural environments.

## ACKNOWLEDGMENTS

The authors would like to thank S. Asher, W. Nelson, H. Sun, and P. Conrad for useful discussions and R. Bhartia for assistance in sample preparation. This work was made possible by a grant from the Director's Research and Development Fund, Jet Propulsion Laboratory, California Institute of Technology and the National Aeronautics and Space Administration Astrobiology Grant.

- <sup>1</sup>M. C. Storrie-Lombardi, A. I. Tsapin, G. D. McDonald, H. Sun, and K. H. Neelson, *ABS PAP Amer. Chem. Soc.* **217**, U844 (1999).
- <sup>2</sup>S. A. Asher, *Anal. Chem.* **65**, 210 (1993).
- <sup>3</sup>P. R. Cary, *Biochemical Applications of Raman and Resonance Raman Spectroscopy* (Academic, New York, 1982).
- <sup>4</sup>J. G. Grasselli and B. J. Bulkin, *Analytical Raman Spectroscopy* (Wiley, New York, 1991).
- <sup>5</sup>S. A. Glazier and H. H. Weetall, *J. Microbiol. Methods* **20**, 23 (1994).
- <sup>6</sup>C. H. Wu and H. L. Warren, *Mycologia* **76**, 1049 (1984).
- <sup>7</sup>S. Determann, J. M. Lobbes, R. Reuter, and J. Rullkotter, *Mar. Chem.* **62**, 137 (1998).
- <sup>8</sup>C. V. Raman and K. S. Krishnan, *Nature (London)* **121**, 501 (1938).
- <sup>9</sup>*Biological Applications of Raman Spectroscopy*, edited by T. G. Spiro (Wiley, New York, 1987), Vol. I-III.
- <sup>10</sup>B. Hudson, *Spectroscopy* **1**, 22 (1986).
- <sup>11</sup>S. A. Overman, M. Tsuboi, and G. J. Thomas, Jr., *J. Mol. Biol.* **259**, 331 (1996).

- <sup>12</sup>M. Tsuboi, S. A. Overman, and G. J. Thomas, Jr., *Biochemistry* **35**, 10403 (1996).
- <sup>13</sup>H. Takeuchi, M. Matsuno, S. A. Overman, and G. J. Thomas, Jr., *J. Am. Chem. Soc.* **118**, 3498 (1996).
- <sup>14</sup>R. Tuma, P. E. Prevelige, Jr., and G. J. Thomas, Jr., *Biochemistry* **35**, 4619 (1996).
- <sup>15</sup>R. Tuma, J. H. K. Bamford, D. H. Bamford, M. P. Russel, and G. J. Thomas, Jr., *J. Mol. Biol.* **257**, 87 (1996).
- <sup>16</sup>R. Tuma, J. H. K. Bamford, D. H. Bamford, and G. J. Thomas, Jr., *J. Mol. Biol.* **257**, 102 (1996).
- <sup>17</sup>T. Li, J. E. Johnson, and G. J. Thomas, Jr., *Biophys. J.* **65**, 1963 (1993).
- <sup>18</sup>K. E. Reilly and G. J. Thomas, Jr., *J. Mol. Biol.* **241**, 68 (1994).
- <sup>19</sup>R. Tuma and G. J. Thomas, Jr., *Biophys. J.* **71**, 3454 (1996).
- <sup>20</sup>A. Wang, B. L. Jolliff, and L. A. Haskin, *J. Geo. Res. Pla.* **100**, 21189 (1995).
- <sup>21</sup>A. Wang, L. A. Haskin, and E. Cortez, *Appl. Spectrosc.* **52**, 477 (1998).
- <sup>22</sup>A. Wang, B. L. Jolliff, and L. A. Haskin, *J. Geophys. Res.* **104**, 27067 (1999).
- <sup>23</sup>S. A. Asher, *Anal. Chem.* **65**, 59 (1993).
- <sup>24</sup>L. Chinsky, H. Hubert-Habart, A. Laigle, and P. Y. Turpin, *J. Raman Spectrosc.* **14**, 322 (1983).
- <sup>25</sup>S. P. A. Fodor, R. P. Rava, T. R. Hayes, and T. G. Spiro, *J. Am. Chem. Soc.* **107**, 1520 (1985).
- <sup>26</sup>M. Ghomi, R. Letellier, E. Taillander, L. Chinsky, A. Laigle, and P. Y. Turpin, *J. Raman Spectrosc.* **17**, 249 (1986).
- <sup>27</sup>Y. Nishimura, M. Tsuboi, W. L. Kubasek, K. Banjor, and W. L. Peticolas, *J. Raman Spectrosc.* **18**, 221 (1987).
- <sup>28</sup>L. Chinsky, B. Jolles, A. Laigle, and P. Y. Turpin, *J. Raman Spectrosc.* **18**, 195 (1987).
- <sup>29</sup>J. R. Perno, C. A. Grygon, and T. G. Spiro, *J. Phys. Chem.* **93**, 5672 (1989).
- <sup>30</sup>C. R. Johnson, M. Ludwig, and S. A. Asher, *J. Am. Chem. Soc.* **108**, 905 (1986).
- <sup>31</sup>S. A. Asher, M. Ludwig, and C. R. Johnson, *J. Am. Chem. Soc.* **108**, 3186 (1986).
- <sup>32</sup>M. Ludwig and S. A. Asher, *J. Am. Chem. Soc.* **110**, 1005 (1988).
- <sup>33</sup>S. P. A. Fodor, R. Copland, C. Grygon, and T. G. Spiro, *J. Am. Chem. Soc.* **111**, 5509 (1989).
- <sup>34</sup>J. Sweeny and S. A. Asher, *J. Phys. Chem.* **94**, 4784 (1990).
- <sup>35</sup>C. Su, Y. Wang, and T. G. Spiro, *J. Raman Spectrosc.* **21**, 8179 (1990).
- <sup>36</sup>S. A. Asher, *Annu. Rev. Phys. Chem.* **39**, 537 (1988).
- <sup>37</sup>R. P. Rava and T. G. Spiro, *Biochemistry* **24**, 1861 (1985).
- <sup>38</sup>S. Hashimoto, S. Ohsaka, H. Takeuchi, and I. Harada, *J. Am. Chem. Soc.* **111**, 8926 (1989).
- <sup>39</sup>G.-Y. Liu, C. A. Grygon, and T. G. Spiro, *Biochemistry* **28**, 5046 (1989).
- <sup>40</sup>R. G. Efremov, A. V. Feofanov, N. N. Modyanov, and I. R. Nabiev, *FEBS Lett.* **260**, 257 (1990).
- <sup>41</sup>J. B. Ames, S. R. Bolton, M. M. Netto, and R. A. Mathies, *J. Am. Chem. Soc.* **112**, 9007 (1990).
- <sup>42</sup>I. Harada, T. Yamagishi, K. Uchida, and H. Takeuchi, *J. Am. Chem. Soc.* **112**, 2443 (1990).
- <sup>43</sup>M. Netto, S. Fodor, and R. Mathies, *Photochem. Photobiol.* **52**, 605 (1991).
- <sup>44</sup>A. Toymana, E. Kurashiki, Y. Watanabe, H. Takeuchi, and I. Harada, *J. Am. Chem. Soc.* **113**, 3615 (1991).
- <sup>45</sup>S. A. Asher, P. J. Larkin, and J. Teraoka, *Biochemistry* **30**, 5944 (1991).
- <sup>46</sup>K. R. Rodgers, C. Su, S. Subramanian, and T. G. Spiro, *J. Am. Chem. Soc.* **114**, 3697 (1992).
- <sup>47</sup>J. Webb, *Phys. Rep.* **60**, 210 (1980).
- <sup>48</sup>L. Furia and O. P. Gandhi, *Phys. Lett. A* **102**, 380 (1984).
- <sup>49</sup>S. Kinoshita, K. Hirata, and T. Kushida, *J. Phys. Soc. Jpn.* **49**, 314 (1980).
- <sup>50</sup>R. A. Dalterio, W. H. Nelson, D. Britt, J. Sperry, D. Psaras, J. F. Tanguay, and S. L. Suib, *Appl. Spectrosc.* **40**, 86 (1986).
- <sup>51</sup>R. A. Dalterio, W. H. Nelson, D. Britt, J. Sperry, D. Psaras, J. F. Tanguay, and S. L. Suib, *Appl. Spectrosc.* **41**, 234 (1987).
- <sup>52</sup>R. A. Dalterio, W. H. Nelson, D. Britt, and J. F. Sperry, *Appl. Spectrosc.* **41**, 417 (1987).
- <sup>53</sup>K. A. Britton, R. A. Dalterio, W. H. Nelson, D. Britt, and J. F. Sperry, *Appl. Spectrosc.* **42**, 782 (1988).
- <sup>54</sup>R. Manoharan, E. Ghiamati, R. A. Dalterio, W. H. Nelson, D. Britt, and J. F. Sperry, *J. Microbiol. Methods* **11**, 1 (1990).
- <sup>55</sup>W. H. Nelson, R. Manoharan, and J. F. Sperry, *Appl. Spectrosc. Rev.* **27**, 67 (1992).
- <sup>56</sup>S. Chadha, R. Manoharan, P. Moenne-Loccoz, W. H. Nelson, W. L. Peti-

- colas, and J. F. Sperry, *Appl. Spectrosc.* **47**, 38 (1993).
- <sup>57</sup>S. Chadha, W. H. Nelson, and J. F. Sperry, *Rev. Sci. Instrum.* **11**, 3088 (1993).
- <sup>58</sup>G. P. Harhay and F. R. Siragusao, *J. Rap. Met. Auto. Micro.* **7**, 25 (1999).
- <sup>59</sup>L. Csillag, M. Janossy, V. Rosa, and T. Salamon, *Phys. Lett. A* **50**, 13 (1974).
- <sup>60</sup>D. C. Gerstenberger, R. Solanki, and G. Collins, *IEEE J. Quantum Electron.* **QE-16**, 820 (1980).
- <sup>61</sup>K. Jain, *Appl. Phys. Lett.* **34**, 398 (1979).
- <sup>62</sup>S. C. Wang, US Patent No. 4,021,845, assigned to Xerox Corp. (3 May 1977).
- <sup>63</sup>K. Venkateswaran, D. P. Moser, and M. E. Dollhopf *et al.*, *Int. J. Syst. Bacter.* **49**, 705 (1999).
- <sup>64</sup>C. R. Stoker and M. A. Bullock *J. Geophys. Res.* **102**, 10881 (1997).
- <sup>65</sup>P. Toulmin, III, A. K. Baird, B. C. Clark, K. Keil, H. J. Rose, Jr., R. P. Christian, P. H. Evans, and W. C. Kelliher, *J. Geophys. Res.* **82**, 4625 (1977).
- <sup>66</sup>L. A. Soderblum and D. B. Wenner, *Icarus* **34**, 622 (1978).
- <sup>67</sup>R. B. Singer, *J. Geophys. Res.* **87**, 10159 (1982).
- <sup>68</sup>Z. Wen, S. A. Overman, and G. J. Thomas, Jr., *Biochemistry* **36**, 7810 (1997).
- <sup>69</sup>J. Ingraham, O. Maaloe, and F. Neidhardt, *The Growth of the Bacterial Cell* (Sinauer, Sunderland, MA, 1983).